CHAPTER VI

THE EFFECT OF BIO COMPATIBLE INHIBITORS ON CORROSION RESISTANCE BEHAVIOUR OF TITANIUM BASED ALLOYS IN SIMULATED BODY FLUID

6.1 Introduction

In the recent times, utilisation of artificial replacement of biological materials (implants) using metals play a remarkable role in the biomedical field[1]. It has been essential for human beings to utilise the implant materials for enhanced and prolonged life[2]. The replacement of implant materials in the body must be chosen based on their biocompatibility and also their influence should not cause deleterious reaction in the body[3]. It is very important that the material must regulate the body conditions and also do not degrade inside the body[4]. The bone materials are artificially replaced by using materials such as metals, ceramics, polymers etc.,. The foremost criteria for choosing artificial implantation is long-term availability without any damage, harmfulness and also need to attain a steady interface between the implanted material and the tissues in the human body. Various bio implantable materials such as Co-Cr, stainless steel alloys etc., have been used. Though Co-Cr alloy possess better mechanical properties, superior resistant to corrosion and it is widely used in construction of prosthesis but unfortunately in biological fluids Co-Cr alloy discharges metal ions resulting in toxicity problem[5]. The usage of stainless steel is due to their cost effectiveness, easy to fabricate, better strength, corrosion and fatigue resistance and was widely implemented in 20^{th} century but failed due to their negative tissue reactions[6]. Among these materials, Ti based alloys are preferable due to their superior property, high melting point, biocompatibility, desired physical properties, high toughness, light weight nature and also the related characteristics like, human bone make Ti to attach the bone cells without any adverse effect and also possible to adapt to the body tissues[7-9]. The tetragonal structure of TiO_2 in Ti implants exhibit a thermodynamically stable oxide layer possessing better corrosion resistance. These excellent properties find Ti alloys in a huge applications including stenosis in human body cavities, cardiovascular stent materials[10], substitution of arthristic hips and knee joints etc.,[11]. It has been reported that every year about 1000 tonnes of Ti devices are implanted for the needy patients throughout the world.

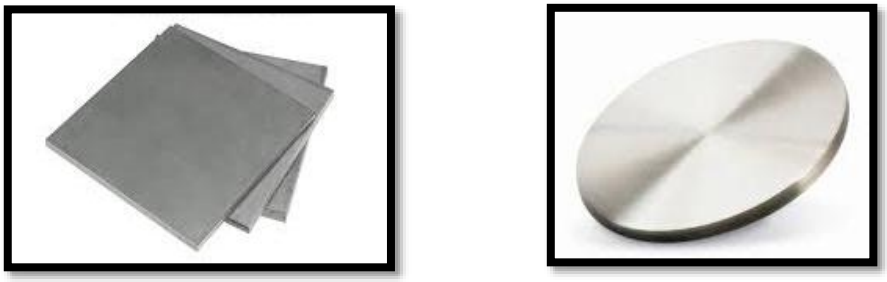

Fig. a: Images of Ti-6Al-4V alloy

Besides the medical applications, Ti alloys are widely used in various fields such as pipelines, petrochemical industries, aerospace, power generation, air foils and air fames[12].

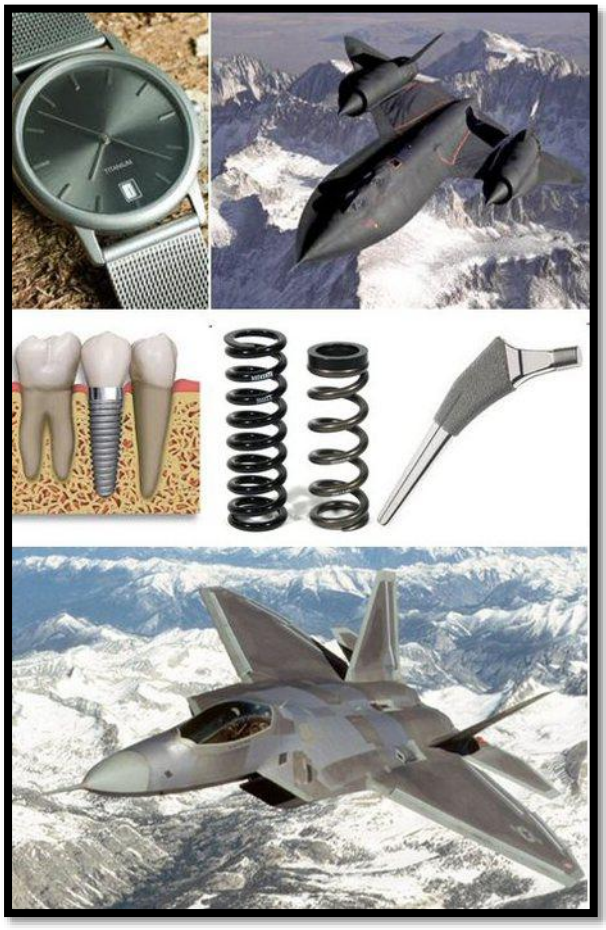

Fig. b: Applications of Ti in various fields

Ti based alloys exhibit anti-corrosive property owing to the protective oxide layer formation of 1- 4 nm thickness on the metal surface[13]. This type of oxide layer is necessary for the contact between the implant material and living tissues which allows excellent

osseointegration process[14]. In general, preparation of Ti-6Al-4V alloy by traditional methods shows a duplex microstructure consisting of α (hcp) phase and β (bcc) phase and also it is possible to modify their properties by altering its microstructure such as bimodal, equiaxed, lameallar under different heat conditions[15]. Despite their wide applications, Ti implants on human body for a prolonged time in the biological fluids having water, dissolved oxygen, protein, plasma, sodium and chloride ions facilitates corrosion[16]. The titanium alloy implants must be protected from being corroded and its life time should be enhanced. This can be achieved by coating the Ti alloy with eco-friendly compounds which prevents deterioration of the alloy.

6.2 Review of literature

Baloyi *et al.*, assessed the improvement in corrosion resistance of base material Ti-6Al-4V using zirconium and zirconia composite material by layer deposition method. An adherent, strong coating of Zr and ZrO_2 phases was obtained. The results revealed an increased hardness of coated Ti-6Al-4V compared to uncoated samples[17].

Graf *et al.*, activated the surface of Ti-6Al-4V alloy using hydroxy apatite nanopowders (HAP) by Q - switched CO_2 laser and O_2, N_2, Ar were used as process gases. It has been found that HAP disclosed a dense and homogeneous microstructure and it was confirmed by X-ray diffraction pattern[18].

Hacisalihoglu *et al.*, studied the tribological properties and electrochemical behaviour of β-type Ti alloys. To understand the structure, mechanical behaviour and surface morphology, XRD and SEM analysis were carried out in SBF solution. Corrosion tests were studied by potentiodynamic polarization techniques. An improvement in corrosion resistance was noticed[19].

Dai *et al.*, performed microstructural analysis and electrochemical studies to analyse the resistivity to corrosion of Ti-6Al-4V alloy in different planes by selective laser melting (SLM) method in 1 M HCl solution. It has been found that XY plane provides superior corrosion resistance than XZ plane. The lesser corrosion resistance of XZ plane was due to the existence of greater α-martensite and lower β-Ti plane in their microstructure[20].

A comparative study of fracture properties of pure Ti and Ti-6Al-4V alloy in simulated biological fluid was carried out by **Marcic *et al*.,.** The results from CTOD (crack tip opening displacement) showed that toughness of Ti-6Al-4V metal samples were superior than pure Ti metal samples[21].

Kandiah *et al*., deposited nanocomposites such as nano-titania, chondroitin -4-sulphate and titania/chondroitin-4-sulphate on Ti-6Al-4V alloy by spin coating method. In order to find the crystalline nature, type of chemical bonding, homogeneity of the surface and composition of the elements, surface characterisation techniques were carried out. The corrosion resistance of Ti-6Al-4V alloy in simulated body fluid in the presence of nanocomposite coating was improved due to increase in the thickness of the passive layer compared to bare Ti-6Al-4V alloy. It has been found that I_{corr} value decreases in presence of coatings. These nanocomposites find application in orthopedics and it was efficient for biommic bone regeneration[22].

Yamaguchi *et al*., studied the influence of surface potential on apatite formation in Ti based alloys subjected to acid and heat treatment. The results revealed that acid and heat treatment enhanced the alloying elements on Ti-6Al-4V, Ti-15Mo-5Zr-3Al, Ti-15Zr-4Nb-4Ta and hence treated alloys can be utilized in orthopedic and dental applications[23].

Ruiz *et al*., studied the dynamical behaviour of corrosion resistance of Ti-6Al-4V alloy by electrochemical noise method. The recurrence plot analysis insisted that the corrosion resistance of Ti-6Al-4V alloy depends on some factors such as electrolyte, in which the metal sample was exposed and sintering type. These factors were important to regulate the conditions required for higher resistance to corrosion of Ti-6Al-4V alloy[24].

Mahdavi *et al*., analysed the influence of TiO_2 nano particles on corrosion resistance of Co-Cr alloys in Hank's solution by EIS measurements. It has been noted that corrosion potential was shifted towards positive side and about 22% decrease in corrosion rate was due to the effect of TiO_2 nanoparticles. The increased value of charge transfer resistance value indicated the better corrosion resistance[25].

Masdek *et al*., evaluated the corrosion behaviour of SS 316L and Ti-6Al-4V in simulated body fluid along with the presence of proteins by electrochemical impedance technique and potentiodynamic polarisation studies. The experimental analysis was carried

out by using different concentrations of 2 to 10% of bovine serum albumin at 37^0C. The results revealed that the corrosion resistance was attained in the presence of proteins containing electrolytes. The high impedance results specified the presence of protein on the surface of the metal[26].

Fekry *et al.,* prepared two composite films namely chitosan nanoparticles and silver nanoparticles containing chitosan nanoparticles and it was coated on the surface of Ti alloy. The corrosion behaviour of the metal surface in artificial saliva solution was understood by EIS and Tafel test. The surface analysis was carried out by SEM-EDAX techniques. It has been found that two chitosan coatings enriched the anti-corrosion property of the metal surface. The anti-bacterial studies were done and it was concluded that the silver nanoparticles with chitosan showed better results than chitosan nanoparticles[27].

Ramirez *et al.,* investigated the influence of addition of aluminium (5-20 at%) on the corrosion nature of Ti-50Ni alloy in simulated body fluid by electrochemical techniques. The addition of Al in low and high levels indicated the microstructure development from columnar to equiaxed grains. These techniques revealed that due to the presence of Al in different levels rate of corrosion reduced to appreciable level. The anti-corrosion property depends on the formation of titanium dioxide layer with duplex structure[28].

Zhang *et al.,* studied the combined effect of H_2O_2 and albumin on corrosion of Ti-6Al-4V alloy in saline solution by electrochemical impedance spectroscopy and potentiodynamic polarisation studies. The polarisation studies indicated that the corrosion behaviour depends on exposure time. It has been found that at short period (24 hours) the albumin reduces the rate of dissolution in the presence of H_2O_2 whereas at longer period (120 hours) it triggers corrosion resulting in the formation of corrosion product layer. EIS studies confirmed the formation of less resistant oxide layer[29].

Hussein *et al.*, analysed the corrosion resistance of nano-grained Ti-20Nb-13Zr in simulated body fluid. Various techniques such as X-ray diffraction, scanning electron microscopy and transmission electron microscopy were employed to understand the phases and microstructural details of the nano material. The corrosion resistivity was studied using electrochemical techniques. SEM analysis predicted the surface morphology. XPS analysis were done to evaluate the formation of protective layer[30].

Gnanavel *et al*., experimented the impact of diamond carbon coating on Ti-6Al-4V and Ti-13Nb-13Zr alloy by electrochemical methods. The coatings were done by hot filament chemical deposition process. Electrochemical studies showed that in SBF solution, diamond carbon coated Ti alloys behaved as an ideal capacitor[31].

Saro *et al*., utilized surface modification route method to enhance the biocompatibility and corrosion resistance of Ti alloy. For surface modification, hydroxyapatite and hydroxyapatite/titanium dioxide coatings were sprayed thermally on Ti-6Al-4V metal substrates. Corrosion analysis were carried out in Ringer's solution by linear polarization and potentiodynamic polarization techniques. To analyse the microstructure X-ray diffraction pattern and SEM- EDS techniques were done. The results revealed that HA coating showed higher biocompatibility than uncoated samples[32].

Buyuksagis *et al*., evaluated the effect of hydroxyapatite coated Ti-6Al-4V alloy on corrosion behaviour. The coating was performed by electrophoresis method. Electrochemical studies were carried out for coated and uncoated samples in simulated body fluid. X-ray diffraction and scanning electron microscope techniques were used to describe the surface nature of the samples[33].

Huang *et al*., reviewed two Ti alloys (Ti-13Nb-13Zr) and (Ti-15Mo) for their mechanical properties and electrochemical behaviour by material testing system and electrochemical measurements in Ringer's solution. The results revealed that Ti-13Nb-13Zr possessed superior corrosion resistivity than Ti-15Mo[34].

The enhancement of corrosion resistance of Ti-6Al-4V by TiO_2 nanotube arrays was analysed by **Sarraf *et al*.,.** A highly crystalline anatase phase with tetragonal symmetry was formed and it was studied by XRD and Raman spectroscopy. A remarkable increased inhibition efficiency was noticed from the corrosion studies[35].

Lu *et al*., adopted sliding friction treatment for coating a nano - grained layer of size less than 100 nm on Ti-6Al-4V alloy. The mechanical properties and electrochemical corrosion behaviour of nanocrystalline Ti-6Al-4V alloy was studied. An enhanced corrosion resistivity was noticed due to the improved stability and thickness of the coated layer. To analyse the mechanical properties tensile experiments were done and results showed high yield strength[36].

Based on the above literature review, it is understood that Ti based alloy is the chief implant material and the metal dissolution rate is retarded by implementing nanomaterials, modifying the surface etc. Hence an attempt was made to analyse the influence of plant extracts on Ti-6Al-4V alloys in simulated biological fluid environment by electrochemical measurements. *Cissus quadrangularis* is a shrub possessing medicinal values and grown in various parts of India, Africa and Srilanka. In ayurveda this particular plant species has been utilized as medicine for fractured patients[37]. It improves bone healing. It has various pharmacological properties such as anti-ulcer, anti-obesity, bone-fracture healing, anti-pyretic, anti-bacterial, anti-tumor etc.,. *Rosa damascena* is a wide spread plant species with several health promoting activities. It has been reported that this species has various pharmacological properties like anti-depressant, anti-oxidant[38], anti-inflammatory etc.,. The chosen plants are non-toxic in nature with pharmacological activities, especially for bone healing hence it was chosen for the present study.

6.3 Experimental details

6.3.1 Preparation of water extracts

Cissus quadrangularis (CQ) and *Rosa damascena* leaves (RD) were collected, cleansed thoroughly with double distilled water to eliminate impurities. After scrubbing, it was dried at room temperature, crumbled to get fine powder sample. To 1 g of the powdered sample added 100 ml of double distilled water, refluxed for 3 hours. It was cooled and filtered using Whattmann filter paper and the filtrate was utilised as inhibitors.

6.3.2 Preparation of metal specimens

Ti-6Al-4V alloy of grade 5 was utilised for the analysis. Before starting the experiment, Ti alloy was manually polished using SiC of different grades, degreased with acetone, air dried and chemically scratched to eliminate oxides using Kroll's reagent.

6.3.3 Preparation of simulated biological fluid (SBF)

The electrolyte utilised for the analysis was simulated physiological fluid, and it was synthetically prepared by using chemical reagents given below and the preparation was based on the previous report[39].

Chemical compounds	Amount in grams
Sodium chloride (NaCl)	8.035
Sodium hydrogen carbonate ($NaHCO_3$)	0.355
Potassium chloride (KCl)	0.225
Dipotassium hydrogenphosphate trihydrate ($K_2HPO_4.3H_2O$)	0.231
Magnesium chloride hexahydrate ($MgCl_2.6H_2O$)	0.311
Calcium chloride ($CaCl_2$)	0.292
Sodium sulfate (Na_2SO_4)	0.072
Tris hydroxyl methyl aminomethane $(HOCH_2)_3CNH_2$	6.118
Hydrochloric acid (HCl)	40 ml

These chemical reagents were taken in a plastic container, kept in the water bath and stirred at a temperature 37.5^{o}C. After confirming the dissolution of the chemical reagents, acid (i.e.,1 M HCl) was added to maintain pH 7.5. Finally, the SBF solution was transferred to the plastic container and kept for further analysis.

6.3.4 Spectral analysis

6.3.4.1 Gas chromatography-mass spectrometry (GC-MS) analysis

The phyto chemical constituents of water extracts of CQ and RD were analysed by using Perkin Elmer Clarus SQ8C. This instrument is a combination of gas chromatograph with mass spectrometer of dimension 30 meters, 0.25 mm ID, 0.25 IM film and DB-5 MS capillary standard non-polar column for analysing the compounds. Helium gas was used as a carrier gas with a constant flow rate of 1 ml/min and 1µl volume of solution was injected and the running time was 30 minutes.

6.3.4.2 Fourier transform-infra red spectroscopy (FT-IR)

IR spectral analysis helps to identify the various functional groups involved in the extracts. IR affinity-SHIMADZU in the frequency range of 4000-400 cm^{-1} was used to record IR spectrum of the water extracts of CQ and RD.

6.3.5 Electrochemical measurements

To acquire knowledge about the corrosion resistivity of Ti-6Al-4V without and with inhibitor electrochemical measurements like open circuit potential, electrochemical impedance spectroscopy, potentiodynamic polarisation studies were carried out using Metroohm autolab instrument with NOVA software. The experiments were proceeded with a three electrode system consisting of platinum as a counter electrode, calomel takes role of reference electrode and Ti-6Al-4V alloy exposure area of 1 cm^2 as a working electrode. The electrolyte (i.e. biological medium) is simulated body fluid (SBF). The impedance studies were done in the frequency range of 10 kHz to 0.01 Hz with amplitude of 10 mV. For the same solution potentiodynamic polarisation studies were carried out in the range of ±200 mV at a scan rate of 1 mV/sec.

6.3.6 Morphological analysis

6.3.6.1 Atomic force microscopy (AFM)

AFM is an accurate, efficient and versatile method for visualising the surface morphology under examination[40]. Ti metal samples were immersed in SBF solution without and with CQ and RD for 3 hours and surface characterization was carried out using NOVA software by multimode scanning probe microscope.

6.3.6.2 Scanning electron microscopy (SEM) and Energy dispersive X-ray spectroscopy (EDS)

The presence of protective layer due to CQWE and RDWE on Ti-6Al-4V alloy was confirmed by immersing the specimen with and without CQWE and RDWE inhibitors in SBF solution for 3 hours. The specimens were removed after the stipulated time and analysed by SEM, the elemental composition was recorded by Energy dispersive X-ray spectroscopy (EDS).

6.4 Results and discussion

6.4.1 Gas chromatography-mass spectrometry (GC-MS) analysis

GC-MS is a versatile tool to find compounds of long and branched chain hydrocarbon, acids, alcohols, volatile matter, esters etc.,[41]. In this study, based on the peak area (%), the

active principle compounds were identified and their retention time, molecular weight, molecular formula and peak area (%) are presented below,

Caption	Compound name	Retention time	Peak area(%)	Molecular weight	Molecular formula
CQWE					
a	Diisooctyl phthalate	29.779	24.999	390.56	$C_{24}H_{38}O_4$
b	Hydroquinone	7.740	19.805	110.11	$C_6H_6O_2$
c	Ethanone, 1-(4-hydroxy-2-methylphenyl)-	8.165	8.822	150.17	$C_9H_{10}O_2$
d	Hexanedioic acid, bis(2-ethylhexyl) ester	27.788	3.840	370.57	$C_{22}H_{42}O_4$
e	Eicosane	20.910	2.930	282.55	$C_{20}H_{42}$
f	6-Hydroxy-4,4,7a-trimethyl-5,6,7,7a-tetrahydrobenzofuran-2(4H)-one	16.214	1.632	196.24	$C_{11}H_{16}O_3$
g	n-Hexadecanoic acid	20.115	1.616	256.42	$C_{16}H_{32}O_2$
RDWE					
a.1	Hydroquinone	7.750	18.946	110.11	$C_6H_6O_2$
b.1	n-Hexadecanoic acid	20.145	4.235	256.42	$C_{16}H_{32}O_2$
c.1	2-Methoxy-4-vinylphenol	8.170	3.792	150.17	$C_9H_{10}O_2$
d.1	Octadeca-9,12-dienoic acid	23.241	2.944	280.45	$C_{18}H_{32}O_2$
e.1	2,3-Dihydro-2,5-dihydroxy-6-methyl-4H-pyran-4-one	5.830	2.801	144.13	$C_6H_8O_4$
f.1	Z-(13,14-Epoxy) tetradec-11-en-1-ol acetate	23.371	2.706	268.39	$C_{16}H_{28}O_3$
g.1	1-Dodecanol,3,7,11-trimethyl	13.357	2.448	228.41	$C_{15}H_{32}O$

The structure of the active compounds is depicted in **Fig. 6.1**. In CQWE diisooctyl phthalate is predominant with peak area (%) of 24.999, where as in RDWE it is hydroquinone with high peak area % of 18.946. On examining the table above it is understood that hydroquinone is present in both CQWE and RDWE almost in same quantities. Moreover, all compounds except eicosane contains oxygen atoms.

6.4.2 Fourier transform-infra red spectroscopy (FT-IR)

IR spectra of water extracts of CQ and RD are presented in **Fig. 6.2**. The bands at 3350, 1660, 1250, 710 cm^{-1} correspond to >OH, >C=O, >C-O, >C-C stretching vibrations in CQWE. The bands at 3400, 2920, 1750, 1625, 1240, 700 cm^{-1} correspond to >OH, >C-H, >C=O, >C=C, >C-O,>C-C stretching vibrations in RDWE.

6.4.3 Electrochemical measurements

6.4.3.1 Open circuit potential (OCP)

OCP determines the nature of the material that undergo electrochemical oxidation in an aggressive medium. The OCP values of Ti-6Al-4V alloy during analysis as a function of time with different concentrations of inhibitor is helpful in analysing the complete (or) partial area inhibition of corrosion and also to assess the concentration revealing the maximum inhibition threshold level[42]. The tendency of the material in presence of inhibitors along with simulated body fluid varies with immersion time. The OCP of Ti-6Al-4V alloy without and with inhibitors of concentrations (2, 6, 12 v/v%) of CQWE and RDWE are depicted in **Fig. 6.3**. A positive displacement of OCP is observed in the presence of inhibitors indicating that inhibitor increases the resistivity to corrosion[43].

6.4.3.2 Electrochemical impedance spectroscopy (EIS)

EIS techniques have been utilised in various corrosion and protection field for evaluating the effectiveness of the inhibitor[44]. It provides knowledge about the corrosion protection mechanism of the inhibitor in terms of adsorbed film. EIS measurements were recorded for Ti-6Al-4V alloy dipped in physiological solution without and with inhibitors of CQWE and RDWE and illustrated in **Fig. 6.4**. Impedance spectra in the form of Nyquist plot was obtained for different concentrations of 2, 6, 12 v/v% of CQWE and RDWE. From **Fig. 6.4** straight line pattern at 45^{o} was noted, indicating diffusion controlled process[45].

It is worthy to note that as the concentration of the inhibitors (CQ and RD) is increased the diffusion pattern also increases leading to duplex dense layer formation consisting of porous layer (external), compact layer (internal) where the internal compact layer actively tends to form a protective barrier to retard the dissolution of metals. It is evident from the **Table 6.1** that the resistance value obtained for inner compact layer is more than the outer porous layer indicating the reduction in corrosion rate owing to TiO_2 passive layer[46]. In Ti-6Al-4V alloy, the inner metal oxide interface contains titanium dioxide (TiO_2), titanium oxide (TiO), titanium(III)oxide enriched with aluminium oxide (Al_2O_3), vanadium oxide (V_2O_3) and vanadium(v) oxide (V_2O_5). The experimental data was fitted and respective equivalent circuit is shown in **Fig. a**

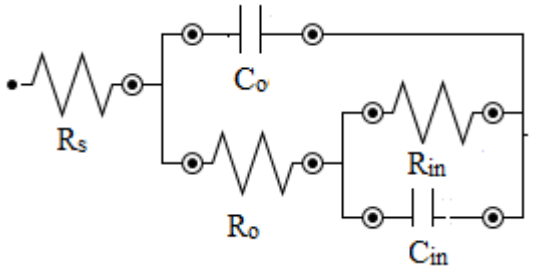

Fig. a: Equivalent circuit

where, R_s - solution resistance, R_o - outer porous layer resistance, R_{in} - inner compact layer resistance, C_o - outer porous layer capacitance, C_{in} - inner compact layer capacitance. In general, V_2O_3 deposited on Ti-6Al-4V start to dissolve slowly which is further enriched by the presence of chloride ions in SBF solution. This behaviour leads to dispersal of vacancies especially in inner oxide layer and dissolution of TiO_2 in water may take place and it is indicated below[47],

$$\{TiO_2\}_{solid} + 2H_2O \longleftrightarrow [Ti(OH)_4]_{aq}$$

$$\{TiO_2\}_{solid} + 2H_2O \longleftrightarrow [Ti(OH)_3]^+_{aq} + OH^-$$

$$\{TiO_2\}_{solid} + 2H_2O \longleftrightarrow [TiO_2OH^-]_{aq} + H_3O^+$$

The passive layer formed on the surface of the metal is unstable leading to release of metal ions in simulated biological fluid. After some time, the passive layer regenerates and the calcium and phosphate ions interact with the TiO_2 surface to form a calcium phosphate layer as shown below,

$$\{Ti\text{-}OH\}_{solid} + Ca^{2+}_{aq} \longleftrightarrow [TiO\text{-}\ldots\ldots\ldots Ca^{2+}(aq)]_{solid} + H^{+}$$

$$\{Ti\text{-}OH\}_{solid} + H_2PO_4^{-}{}_{aq} \longleftrightarrow [Ti\ldots\ldots H_2PO_4(aq)]_{solid} + OH^{-}_{aq}$$

$$3Ca^{2+}_{(aq)} + 2PO_4^{3-}{}_{(aq)} \longleftrightarrow \{Ca_3(PO_4)_2\}_{solid}$$

The above reactions not only indicate the effect of cations (Ca^{2+}) on the surface of Ti alloys but also specifies the exchange of basic hydroxide anions (OH^-) with phosphate anions to form a calcium phosphate layer. Moreover, as inhibitor is added they may synergistically react with adsorbed calcium and phosphate ions, diffuse into the cavities of the inner layer thus averting the dissolution of metal process. The impedance value of solution resistance (inhibitor) in **Table 6.1** is high compared to that of SBF without inhibitor indicating that CQWE and RDWE inhibitors has a tendency to reduce the leakage of metal ions into the electrolyte. Furthermore, decrease in C_{in} value of the inhibitor from blank (8.52 μFcm^2) also evinced that the diffusion of corrosive ions reaching the metal surface is reduced thus mitigating the metal dissolution[48].

6.4.3.3 Polarisation studies

In order to analyse the influence of green inhibitors on corrosion resistance of Ti-6Al-4V, Tafel curves were recorded in SBF solution with varying concentrations of 2, 6, 12 v/v% of CQWE and RDWE and corresponding plots are presented in **Fig. 6.5**. From the Tafel plots, important parameters like corrosion current density (I_{corr}), corrosion potential (E_{corr}) as well as Tafel plots (b_a and b_c) were found and tabulated in **Table 6.2**. On observing **Table 6.2** it is understood that I_{corr} value of the inhibitors (CQWE and RDWE) decreased compared to that of blank. It indicates that inhibitor contains hetero atoms like oxygen, aromatic compounds etc., capable to adsorb on the metal surface thus retarding the exposure of the surface to corrosion[49]. The exposure of the metallic surface towards the corrosive media is reduced due to the presence of CQWE and RDWE inhibitors. Moreover, the inhibitors are more efficient to reduce the corrosion rate by forming a protective barrier film, mainly due to the increased thickness as well as the density of the passive film[50]. The inhibitor has a tendency to enhance the passivation properties of Ti-metal surface[51]. Thus the improved passive layer increases the corrosion resistance by reducing the exposure of the surface to aggressive medium. Based on assumption following reactions may occur as Ti alloy exposed to SBF.

- The presence of Ti^{4+} due to reaction of Ti and TiO_2 produces more number of metal ions and electrons inside the oxide as per the following reactions. These excessive charges have the tendency to move in the zone of lattices of metal and dispersed outside the oxide.

$$Ti \longleftrightarrow Ti^{4+} + 4e^-$$

- As soon as the Ti^{4+} reaches the interface of the oxide film and simulated body fluid, chloride ions in electrolyte readily combine with metal ions and produce alkali chloride which is soluble and it again reaches the electrolyte. It is due to strong oxidising capacity of chloride preferentially make it to adsorb on the film[52].

$$Ti^{4+}_{ox} + Cl^-_{aq} + H_2O \longrightarrow [Ti.Cl.OH]^{2+}_{ox} + H^+_{aq}$$

$$[Ti.Cl.OH]^{2+}_{ox} \longrightarrow [Ti.Cl.OH]^{2+}_{aq}$$

$$[Ti.Cl.OH]^{2+}_{aq} + 2H_2O \longrightarrow [Ti(OH)_3]Cl + 2H^+_{aq}$$

It is clearly understood from the electrochemical studies that inhibitor plays a dominant role by adsorbing on the metal surface thereby increasing the surface coverage so that the intrusion of Ti^{4+} ions into electrolyte is reduced which in turn decreases the metal dissolution in SBF solution.

6.4.4 Surface analysis

6.4.4.1 Atomic force microscopy (AFM)

AFM images for Ti-6Al-4V alloy in simulated body fluid without and with CQWE and RDWE are shown in **Fig. 6.6**. A rough surface was observed in blank metal specimen (**Fig. 6.6a**) whereas roughness reduced in the presence of inhibitors (CQWE and RDWE). This is also confirmed from the average roughness value of blank 73.368 nm whereas for CQWE 34.017 nm and RDWE 23.552 nm the reduction in roughness evinced the adsorption of the inhibitor on the metal surface.

6.4.4.2 Scanning electron microscopy (SEM) and Energy dispersive X-ray spectroscopy (EDS)

SEM images were recorded for Ti-6Al-4V alloy in uninhibited and inhibited solution of CQWE and RDWE and presented in **Fig. 6.7**. It can be observed from **Fig. 6.7a** Ti alloy without inhibitor showed a mild dissolution of the metal represented in the form

of rough surface. On the other hand, in the presence of inhibitor, the localised corrosion is reduced as evident from **Figs. 6.7b and c** owing to the formation of protective layer and this layer decreases the contact of metal and aggressive medium. The elemental composition was presented in **Table 6.3**. The EDS spectra in the presence of inhibitor shows additional peaks also evident for the tendency of green inhibitor to adsorb on the metal surface.

6.5 Conclusions

Based on the above results it can be concluded that,

- Electrochemical impedance spectroscopy revealed the significance of corrosion resistance by internal compact layer. Furthermore, addition of inhibitors increases the value of R_{in}.
- From polarisation measurements it is evident that I_{corr} decreases as inhibitor is added is related to decrease in metal dissolution.
- Both the inhibitors CQWE and RDWE acted as a better inhibitor to reduce the dissolution of metal.

6.6 References

1. M.T. Mohammed, Z.A. Khan, A.N. Siddiquee, Procedia. Mat. Sci., **6** (2014) 1610.
2. Y.H. Li, C. Yang, H.D. Zhao, S.G. Qu, X.Q. Li, Y.Y. Li, Materials., **7** (2014) 1709.
3. J. Prikrylova, J. Prochazkova, S. Podzimek, Biomed Res. Int., (2019) https://doi. org /10.1155/2019/2519205.
4. H.R.A. Bidhendi, M. Pouranvari, Metalurgija - MJoM., **17** (2011) 13.
5. C.L. Melendez, E.M.G. Ochoa, M.I.F. Zamora, R.G.B. Margulis, C.C. Gallardo, C.P.C. Morquecho, J.G.C. Nava, A. Villafane, Int. J. Electrochem. Sci., **7** (2012) 1160.
6. L.C. Zhang, L.Y. Chen, Adv. Eng. Mater., (2019) https://doi.org /10.1002/adem. 201801215.
7. S.L. Assis, S. Wolynee, I. Costa, Electrochim. Acta., **51** (2006) 1815.
8. S. Hohn, S. Viratanen, App. Surf. Sci., **329** (2015) 356.
9. S.H. Chen, S.C. Ho, C.H. Chang, C.C. Chen, W.C. Say, Surf. Coat. Technol., **302** (2016) 215.
10. Y.X. Tian, Z. T. Yu. C. Y.A. Ong, D. Kent, G. Wang, J. Mech. Behav. Biomed. Mater., **45** (2015)132.
11. R. Gaddam, R. Pederson, M. Hornqvist, Anti. Corros. Sci., **78** (2014) 378.
12. C.E.B. Marino, S.R. Biaggio, R.C.R. Filho, N. Bocchi, Electrochim. Acta., **51** (2006) 6580.
13. C.E.B. Marino, E.M. Oliveira, R.C.R. Filho, S.R. Biaggio, Corros. Sci., **43** (2001) 1465.
14. T. Hanawa, Front. Bioeng. Biotechnol., (2019) https://doi.org/10.3389/fbioe. 2019.00170.
15. V.A. Alves, R.Q. Reis, I.C.B. Santos, D.G. Souza, T.D.F. Goncalves, M.A. P.Silva, A. Rossi, L.A.D. Silva, Corros. Sci., **51** (2009) 2473.
16. E. Mohsen, E. Zalnezhad, A.R. Bushroa, A.M. Hamouda, B.T. Goh, G.H. Yaoon, Ceram. Int., **41** (2015) 14447.

17. N.M. Baloyi, A.P.I. Popoola, S.L. Pityana, SAJIE., **25** (2014) 62.

18. S. Graf, F.A. Muller, J. Ceram. Sci. Tech., **5** (2014) 281.

19. I. Hacisalihoglu, A. Samancioglu, F.Yildiz, G. Purcek, A. Alsaran, Wear., **333** (2015) 679.

20. N. Dai, L. Zhang, J. Zhang, X. Zhang, N. Oingzhao, Y. Chen, C. Yang, Corros. Sci., **111** (2016) 703.

21. S. Marcic, A. Praunseis, JET., **9** (2016) 55.

22. K. Kandiah, N. Duraisamy, B. Ramaswamy, IET., (2017) DOI:10.1049/iet-nbt. 2017.0160.

23. S.Yamaguchi, H. Hashimoto, R. Nakai, H. Takadama, Materials., **10** (2017) 1127.

24. J.C.B. Ruiz, C. Lerma, C.G.N. Dino, R.G.B. Margulis, R.R.T. Knight, Int. J. Electrochem. Sci., **13** (2018) 2585.

25. S. Mahdavi, S.R. Allahkaram, M. Adabi, Nanomed. Res. J., **3** (2018) 154.

26. N.R.N. Masdek, A.A. Rozali, M.C. Murad, Z. Salleh, ISIJ International., **58** (2018) 1519.

27. A.M. Fekry, M.S. Hussein, Egypt. J. Chem., **61** (2018) 747.

28. M.J.G. Ramirez, R.L. Sesenes, I.R. Cadena, J.G.G. Rodriguez, J. Mater. Res. Technol., **7** (2018) 223.

29. Y. Zhang, O. Addison, F. Yu, B.C.R. Troconis, J.R. Scully, A.J. Davenport, Sci. reports, (2018) Doi:10.1038/s41598-018-21332.

30. M.A. Hussein, M. Kumar, R. Drew, N.A. Aqeeli, Materials., **11** (2018) 1.

31. S. Gnanavel, S. Ponnusamy, L. Mohan, R. Radhika, C. Muthamizhchelvan, K. Ramasubramanian, JMEPEG., **27** (2018) 1635.

32. T.P.S. Sarao, H. Singh, J. Therm. Spray. Techn., **27** (2018) 1388.

33. A. Buyuksagis, Y. Kayali, AKU J. Sci. Eng., **18** (2018) 807.

34. C.L. Huang, T.H. Chen, C.C. Chiang, S.Y. Lin, Int. J. Electrochem. Sci., **13** (2018) 2779.

35. M. Sarraf, N.L. Sukiman, A.R. Bushroa, B.N. Tabrizi, A. Dabbagh, N.H.A. Kasim, W.J. Basirum, J. Aust. Ceram. Soc., **55** (2019) 187.

36. J. Lu, W. Zhang, W. Huo, Y. Zhao, W.Cui, Y. Zhang, Materials., **12** (2019) 760.

37. H.R. Brahmkshatriya, K.A. Shah, G.B. Ananthkumar, M.H. Brahmkshatriya, Ayu., **36** (2015) 169.

38. P.S. Patil, P.A. Tatke, S.Y. Gabhe, AJPCT., **3** (2015) 589.

39. T. Kokubo, H. Takadama, Biomaterials., **27** (2006) 2907.

40. K.M. Shainy, P.R. Ammal, K.N. Unni, S. Benjamin, A. Joseph, J. Bio. Tribo. Corros., **2** (2016) DOI 10.1007/s40735-016-0050-3.

41. M.S. Rukshana, A. Doss, T.P.K. Pushparani, Asian. J. Plant. Sci. Res., **7** (2017) 9.

42. Q.A. Yousif, A.A. Al-Zhara, ARPN-JEAS., **11** (2016) 12619.

43. J.C.M. Rosca, E.D.H. Santana, S. Drob, A.M. Ortigosa, Mater. Res. Soc. Symp. Proc., **1355 (**2011) DOI:10.1557/opl.2011.1137.

44. D.T. Orkega, T. Pandian, E.M.G. Ochoa, Mat. Sci., **13** (2007)163.

45. M.J.G. Ramirez, R.L. Sesenes, I.R. Cadena, J.G.G. Rodriguez, J. Mater. Res. Technol., (2017) https://doi.org/10.1016/j.jmrt.2017.07.003.

46. I. Milosev, T. Kosec, H.H. Strehblow, Electrochim. Acta., **53** (2008) 3547.

47. S. Tamilselvi, V. Raman, N. Rajendran, Electrochim. Acta., **52** (2006) 839.

48. A. Petchiammal, S. Selvaraj, K. Kalirajan, IJRRAS., **3** (2014) 88.

49. F. Contu, B. Elsener, H. Bohni, Corros. Sci., **46** (2004) 2241.

50. N.R.N. Masdek, A.A. Rozali, M.C. Murad, Z. Salleh, ISIJ International., **58** (2018) 1519.

51. J. Hu, L. Chen, X. Zhong, S. Yu, Z. Zhang, D. Zeng, T. Shi, Int. J. Electrochem. Sci., **12** (2017) 8878.

52. X. Zhang, S. Yu, Z. He, Y. Liu, Corros. Sci. Prot. Technol., **15** (2003) 249.

Table 6.1: AC-impedance parameters for the corrosion of Ti-6Al-4V alloy for varying concentrations of CQWE and RDWE in simulated body fluid

Inhibitor	Conc. (v/v %)	R_s (Ω cm^2)	R_o (KΩ cm^2)	C_o (μF/cm^2)	n_o	R_{in} (KΩ cm^2)	C_{in} (μF/cm^2)	n_{in}
BLANK		13.22	3.842	9.64	0.803	3.922	8.52	0.815
CQWE	2	14.62	4.002	9.11	0.736	4.412	8.16	0.729
	6	15.83	5.115	8.55	0.812	5.685	7.29	0.833
	12	17.64	7.048	7.13	0.854	8.039	6.08	0.898
RDWE	2	15.56	5.102	8.67	0.805	5.269	8.09	0.861
	6	18.02	6.924	7.29	0.848	7.187	6.62	0.892
	12	18.96	7.813	6.58	0.906	8.795	5.83	0.911

Table 6.2: Potentiodynamic polarisation parameters for the corrosion of Ti-6Al-4V alloy for varying concentrations of CQWE and RDWE in simulated body fluid

Inhibitor	Conc. (v/v %)	Tafel slopes (mV/dec)		$-E_{corr}$ (mV)	I_{corr} (μA/cm^2)
		b_a	b_c		
BLANK	-	46	124	477.5	$2.00x10^{-1}$
CQWE	2	19	148	493.3	$2.92x10^{-2}$
	6	23	133	485.6	$2.43x10^{-2}$
	12	28	119	487.3	$1.96x10^{-2}$
RDWE	2	85	172	434.0	$2.26x10^{-2}$
	6	103	134	399.8	$5.66x10^{-3}$
	12	162	146	390.4	$4.11x10^{-3}$

Table 6.3: Composition of elements in uninhibited and inhibited metal specimen

Element	Ti-6Al-4V alloy	CQWE	RDWE
Ti	68.12	52.22	51.54
V	1.54	0.56	0.58
Al	22.11	17.44	17.23
Si	8.23	4.11	3.22
Mg	-	0.6	0.62
K	-	0.08	0.085
Ca	-	0. 09	0.105
C	-	15.66	16.54
O	-	9.24	10.08

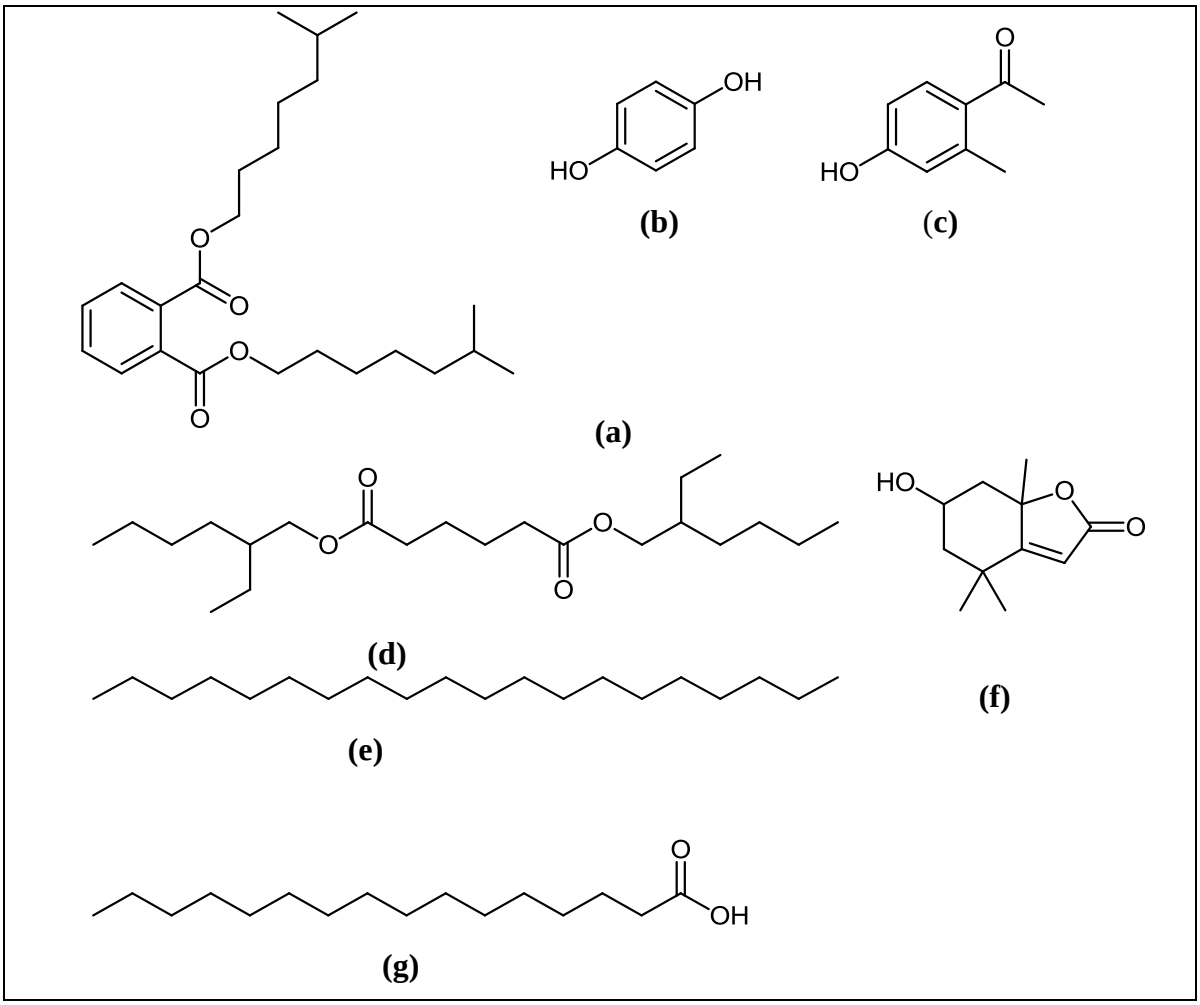

Fig. 6.1(a): Structure of predominant compounds in CQWE

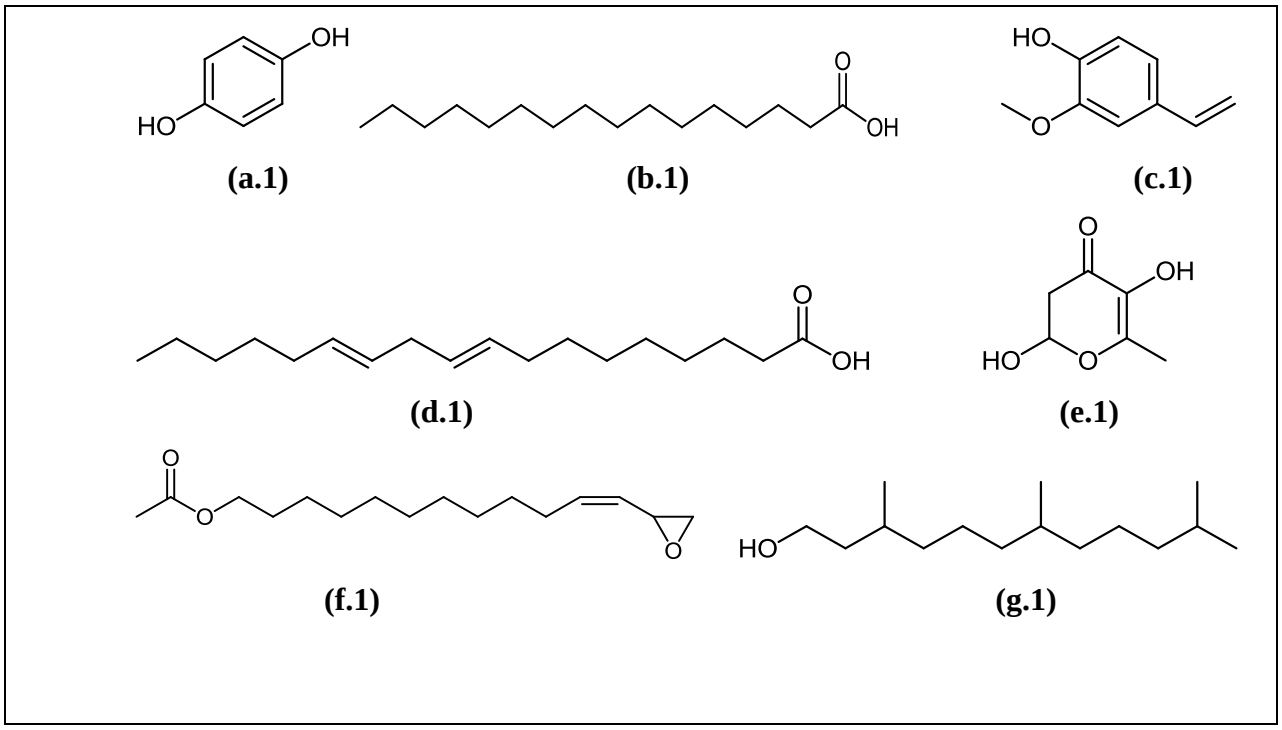

Fig. 6.1(b): Structure of predominant compounds in RDWE

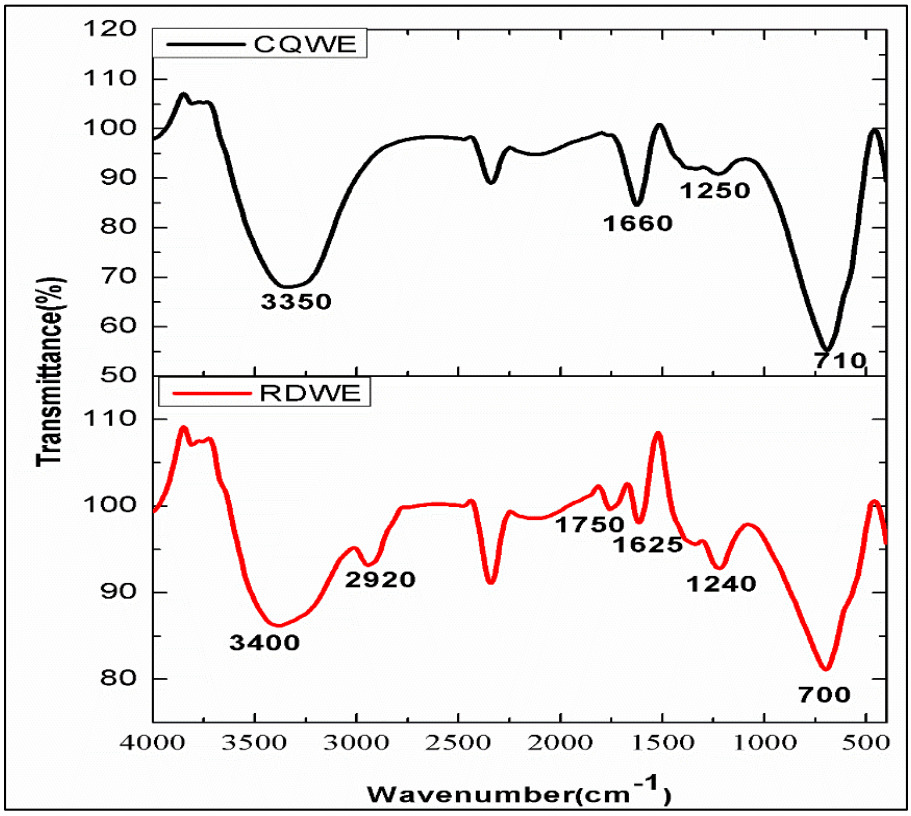

Fig. 6.2: IR spectrum of CQWE and RDWE extracts

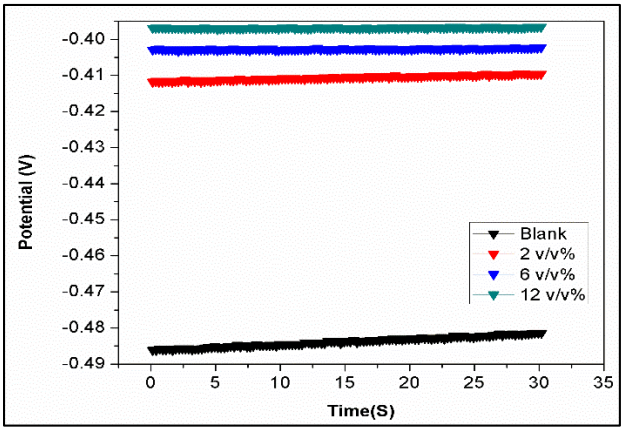

Fig. 6.3(a): OCP plots for Ti-6Al-4V alloy in simulated body fluid without and with different concentrations of CQWE

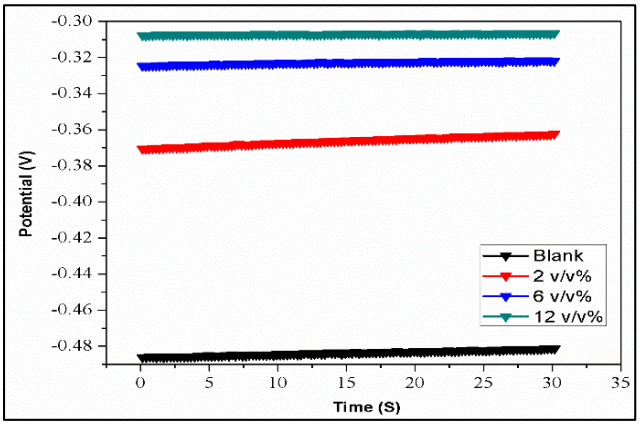

Fig. 6.3(b): OCP plots for Ti-6Al-4V alloy in simulated body fluid without and with different concentrations of RDWE

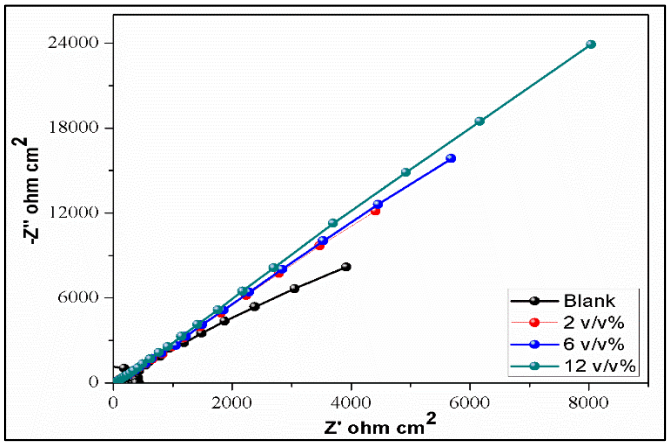

Fig. 6.4(a): Nyquist plots for Ti-6Al-4V alloy in simulated body fluid without and with different concentrations of CQWE

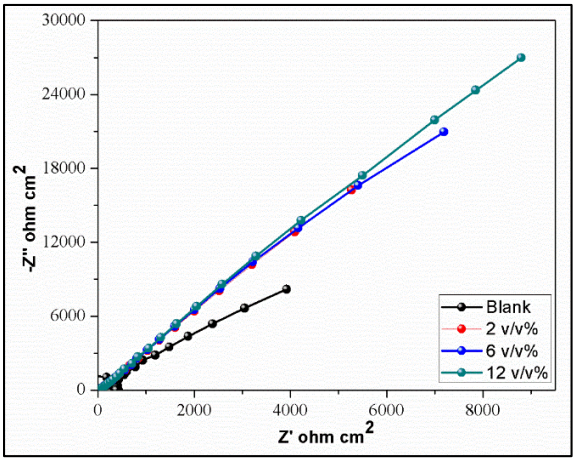

Fig. 6.4(b): Nyquist plots for Ti-6Al-4V alloy in simulated body fluid without and with different concentrations of RDWE

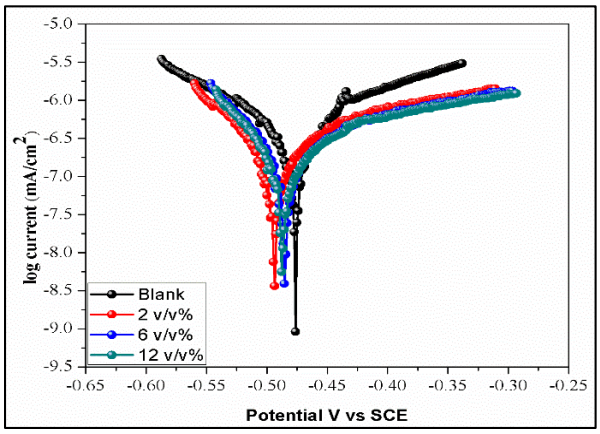

Fig. 6.5(a): Tafel plots for Ti-6Al-4V alloy in simulated body fluid without and with different concentrations of CQWE

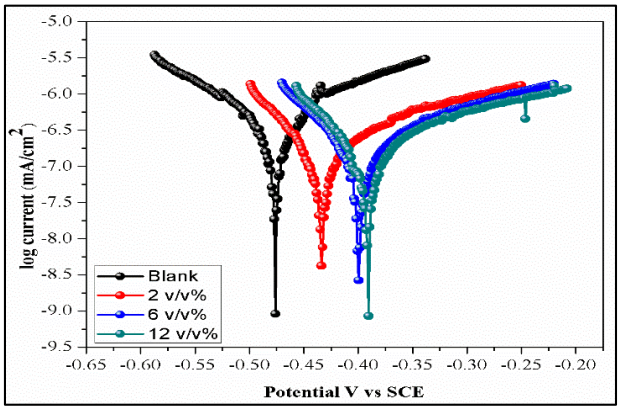

Fig. 6.5(b): Tafel plots for Ti-6Al-4V alloy in simulated body fluid without and with different concentrations of RDWE

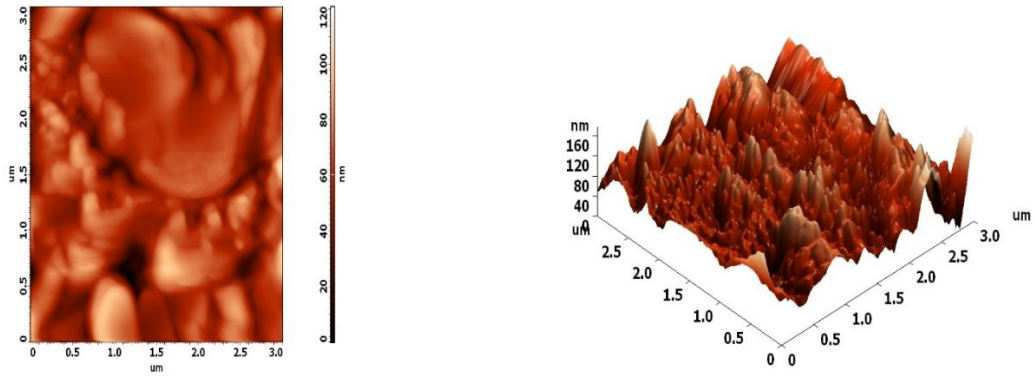

(a)

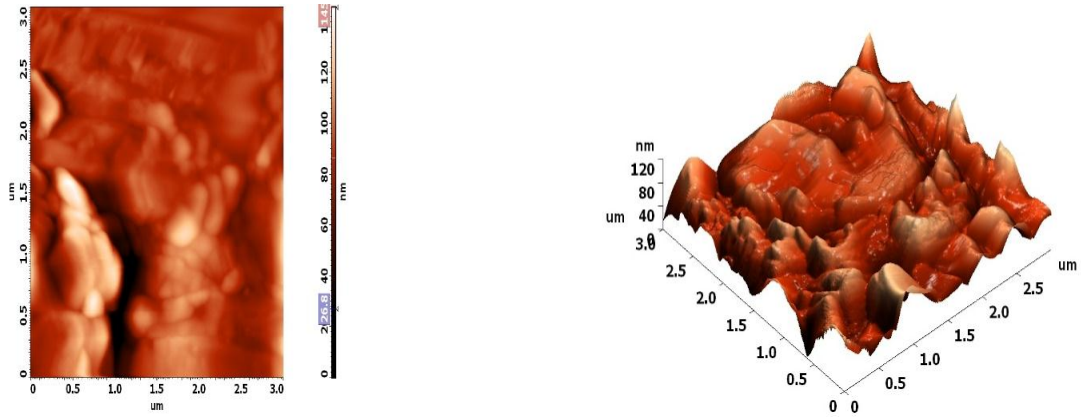

(b)

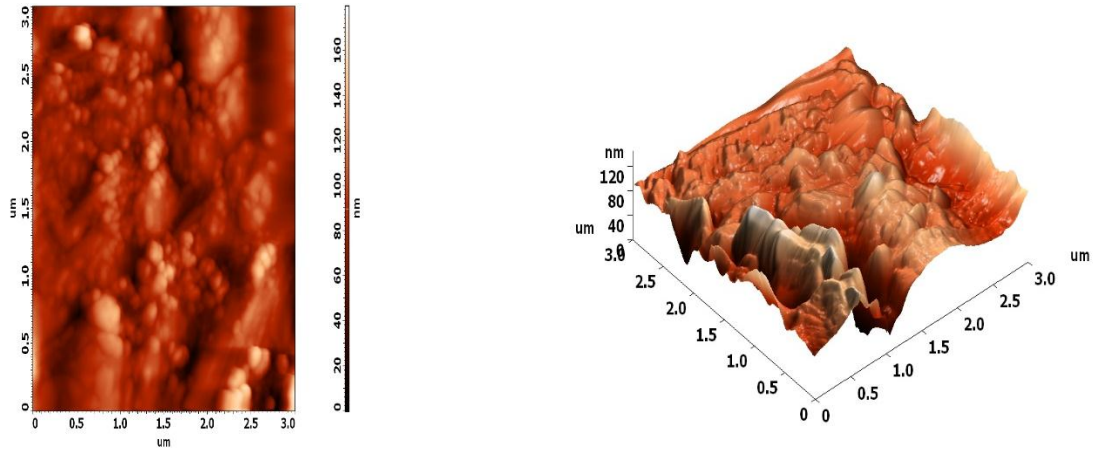

(c)

Fig. 6.6: AFM images in 2D and 3D view for Ti-6Al-4V alloy in simulated body fluid (a) blank (b) CQWE (c) RDWE

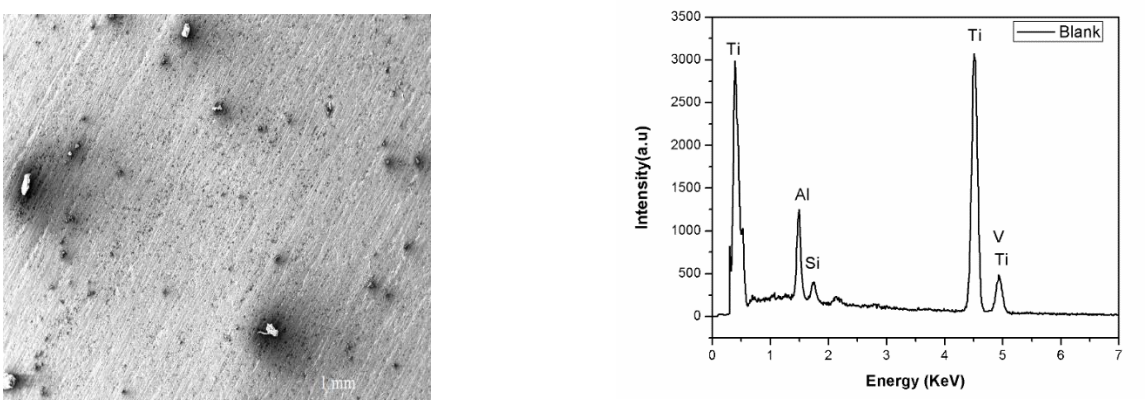

(a)

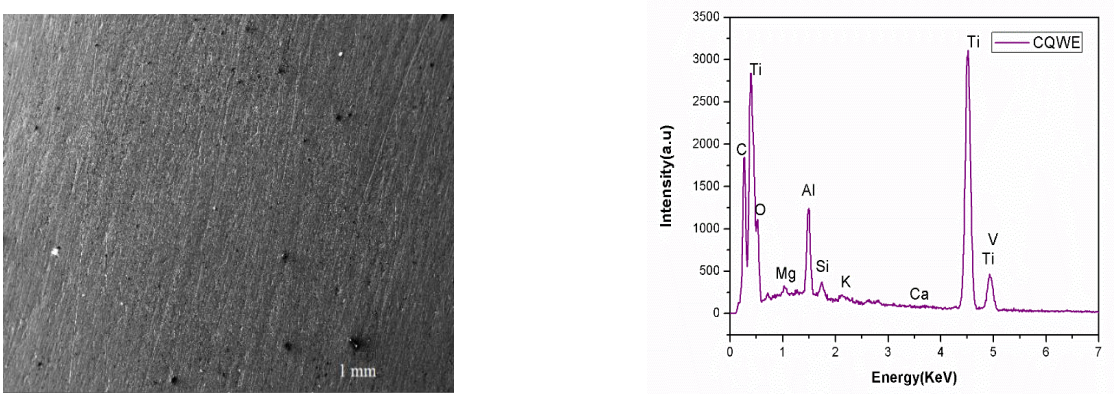

(b)

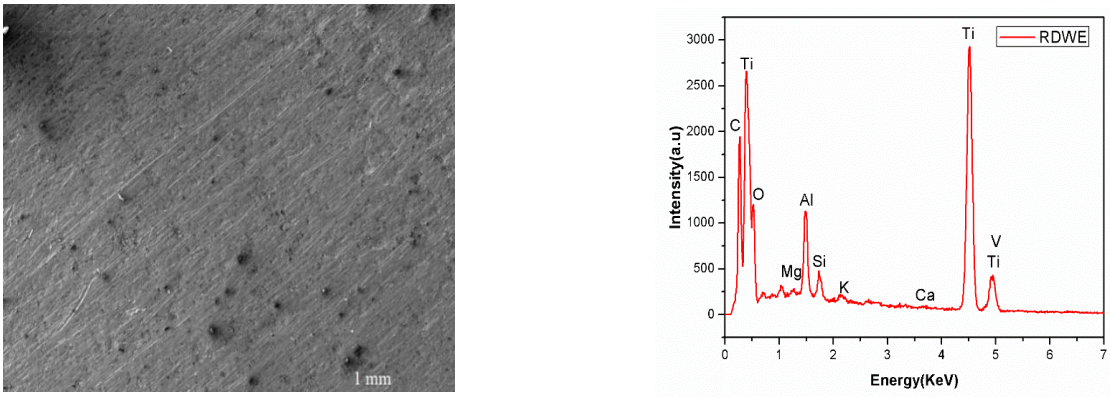

(c)

Fig. 6.7: SEM- EDS for Ti-6Al-4V alloy in simulated body fluid

(a) blank (b) CQWE (c) RDWE